Cranial Nerve Schwannomas: Diagnostic Imaging Approach[1]

Aaron D. Skolnik, MD
Laurie A. Loevner, MD
Deepak M. Sampathu, MD, PhD
Jason G. Newman, MD
John Y. Lee, MD
Linda J. Bagley, MD
Kim O. Learned, MD

Abbreviations: CN = cranial nerve, CN I = olfactory nerve, CN II = optic nerve, CN III = oculomotor nerve, CN IV = trochlear nerve, CN V = trigeminal nerve, CN VI = abducens nerve, CN VII = facial nerve, CN VIII = vestibulocochlear nerve, CN IX = glossopharyngeal nerve, CN X = vagus nerve, CN XI = accessory nerve, CN XII = hypoglossal nerve, CPA = cerebellopontine angle, IAC = internal auditory canal, ICA = internal carotid artery

SA-CME LEARNING OBJECTIVES

After completing this journal-based SA-CME activity, participants will be able to:

■ Recognize the imaging features of CN schwannomas.

■ Perform a targeted evaluation of the anatomy along the course of appropriate CNs.

■ Correlate the CN origins of schwannomas with the associated clinical presentations and evidence of end-organ compromise.

See www.rsna.org/education/search/RG.

Schwannomas are benign nerve sheath tumors that may arise along the complex course of the cranial nerves (CNs), anywhere in the head and neck. Sound knowledge of the CN anatomy and imaging features of schwannomas is paramount for making the correct diagnosis. In this article, we review approaches to diagnosing CN schwannomas by describing their imaging characteristics and the associated clinical presentations. Relevant anatomic considerations are highlighted by using illustrative examples and key differential diagnoses categorized according to regions, which include the anterior skull base, orbit, cavernous sinus, basal cisterns, and neck. The clinical presentations associated with CN schwannomas vary and range from no symptoms to symptoms caused by mass effect or CN deficits. Individuals with the inherited disorder neurofibromatosis type 2 are predisposed to multiple schwannomas. When a lesion follows the course of a CN, the radiologist's roles are to confirm the imaging features of schwannoma and exclude appropriate differential considerations. The characteristic imaging features of CN schwannomas reflect their slow growth as benign neoplasms and include circumscribed margins, displacement of local structures, and smooth expansion of osseous foramina. These neoplasms exhibit various degrees of solid enhancement, often with internal cystic spaces on magnetic resonance (MR) and computed tomographic (CT) images and heterogeneous high signal intensity specifically on T2-weighted MR images. Clinical and/or imaging evidence of end-organ compromise of the involved CN may exist and aid in the identification of the nerve of origin. With a detailed understanding of the course of the CNs, the diagnostic features of CN schwannomas, and the correlation between these data and the associated clinical presentations of these tumors, the radiologist can have a key role in the diagnosis of CN schwannomas and the treatment planning for affected patients.

©RSNA, 2016 • *radiographics.rsna.org*

Introduction

A schwannoma is a benign nerve sheath tumor composed of spindle cells in a variably compact (Antoni type A neurilemoma pattern) or loose (Antoni type B neurilemoma pattern) organization (1). This tumor may arise along the course of any nerve sheath of the peripheral nerves or cranial nerves (CNs); however, its prevalence varies among these nerves. Intracranial schwannomas have rarely been reported without association to a CN (2). The majority (approximately 90%) of CN schwannomas arise from the vestibulocochlear nerve (CN VIII), with the next most commonly involved nerves being the trigeminal (CN V) and facial (CN VII) nerves, followed by the lower CNs, which include the glossopharyngeal (CN IX), vagus (CN X), accessory (CN XI), and hypoglossal (CN XII) nerves (3). Although most of these tumors arise sporadically, individuals with the genetic condition neurofibromatosis

TEACHING POINTS

- On T2-weighted images, schwannomas appear heterogeneously hyperintense. This heterogeneity is attributed to regions of compactly arranged cells (Antoni type A) mixed with regions of loosely arranged cells (Antoni type B), with variable cellularity and water content.

- Both MR and CT images show evidence of the slow growth of schwannomas, including smooth expansion of the neural foramina, osseous remodeling, and/or deformation of adjacent brain tissue, with a disproportionately small amount of edema, given the size of the lesion.

- The diagnostic approach for a patient with diplopia involves evaluation for CN schwannoma not only in the orbit and cavernous sinus but also in the interpeduncular, ambient, and prepontine cisterns and Dorello canal.

- Although CN VII and CN VIII schwannomas may have identical imaging appearances if they are confined to the CPA-IAC complex, it is important to evaluate the findings for extended enhancement or expansion of the labyrinthine segment and geniculate ganglion of CN VII, as this is a subtle clue to a CN VII rather than CN VIII origin.

- Although CNs IX–XII all course through the upper suprahyoid carotid space at the level of the nasopharynx, only CN X continues farther inferiorly in the infrahyoid carotid space. Therefore, an infrahyoid carotid space schwannoma can be attributed to a CN X origin.

type 2 are predisposed to these neoplasms. Neurofibromatosis type 2 is also known as multiple inherited schwannomas, meningiomas, and ependymomas syndrome, which describes the tumors to which these individuals are genetically predisposed. Persons with neurofibromatosis type 2 characteristically develop bilateral vestibular schwannomas, but approximately half of them also have nonvestibular schwannomas, which most commonly involve the oculomotor nerve (CN III) and CN V (4). Individuals who have schwannomatosis, a similar disorder, have a genetic predisposition to develop schwannomas (5).

In this article, the imaging features of CN schwannomas and the common associated clinical presentations are reviewed, with relevant anatomic considerations and illustrative examples of schwannomas highlighted according to regions, which include the anterior cranial fossa, orbit, cavernous sinus, cisterns, temporal bone, and extracranial head and neck regions. Key differential diagnostic considerations based on anatomic region, as well as helpful differentiating features, are also described (Table 1).

Imaging Features

To diagnose CN schwannoma, a detailed understanding of the complex anatomic courses of the CNs is first required. The CNs are becoming increasingly more visible owing to modern imaging techniques such as steady-state free precession

and three-dimensional balanced fast field-echo magnetic resonance (MR) imaging (6–8). Knowledge of the CN anatomy enables recognition of the lesions that follow the course of the CNs; then, analysis of the imaging features can guide the clinician in making the appropriate diagnosis.

Schwannomas have a characteristic appearance at MR imaging (Table 2). On T2-weighted images, schwannomas appear heterogeneously hyperintense. This heterogeneity is attributed to regions of compactly arranged cells (Antoni type A) mixed with regions of loosely arranged cells (Antoni type B), with variable cellularity and water content (1,9). The "target sign" appearance of peripheral high signal intensity and central low signal intensity in peripheral nerve schwannomas on T2-weighted images has been described and is reportedly highly specific but insensitive (9). In our experience, the target sign is rarely seen at imaging of CN schwannoma. On T1-weighted images, these lesions have low or intermediate signal intensity and demonstrate avid enhancement after contrast material administration, with or without nonenhancing cystic spaces (Fig 1). Larger lesions commonly have heterogeneous enhancement, cystic spaces, and foci of hemosiderin due to internal hemorrhage (Fig 1) (10). Gradient-recalled-echo and susceptibility-weighted MR images may have susceptibility artifacts if hemorrhage is present, and although large intratumoral hemorrhage is rarely seen, intratumoral microhemorrhage is common in CN schwannomas (10,11).

At CT, CN schwannomas demonstrate low to intermediate attenuation, with variable enhancement (12,13). Both MR and CT images show evidence of the slow growth of schwannomas, including smooth expansion of the neural foramina, osseous remodeling, and/or deformation of adjacent brain tissue, with a disproportionately small amount of edema, given the size of the lesion (Fig 1) (12,14,15). In the neck, these lesions also displace adjacent structures without invasion—as in the case of a CN X schwannoma splaying the ICA and internal jugular vein in the carotid space (Fig 2), without narrowing or occluding the vessel (16,17).

When the imaging features and clinical signs are compatible with schwannoma, the presence of end-organ compromise such as denervation-induced muscle atrophy or sensory deficit may aid in the identification of the CN of origin. The presence of this disorder can also aid clinicians in assessing the risk of a CN deficit related to treatment (18,19). Although the ancillary finding of end-organ compromise may be helpful, two caveats should be kept in mind: First, the schwannoma may compromise not only the CN of origin but also an adjacent

Table 1: Region-based Common Differential Diagnoses for CN Schwannomas

Region	Involved CNs*	Common Differential Diagnoses	Distinguishing Features
Anterior cranial fossa, nasal cavity	I	Meningioma	Enhancing dural tail
		Nasal cavity carcinomas, esthesioneuroblastoma	Bone destruction, invasion of orbit or brain
Intraorbital region	II–VI	Cavernous malformation	Point or regional spreading enhancement
		Venolymphatic malformation, varix	...
		Perineural spread of neoplasm	...
Cavernous sinus	III–VI	Meningioma	Possible narrowing of cavernous ICA, enhancing dural tail
		Perineural spread of neoplasm	...
		Lymphoma	...
		Aneurysm	Vascular flow void
Cisterns	I–XII	Leptomeningeal disease (tumor, sarcoidosis)	Involves multiple nerves and other meningeal surfaces
Temporal bone	VII	Hemangioma	Involves the geniculate fossa, has irregular borders with intralesional stippled calcifications
		Cholesteatoma	Lytic lesion
		Metastasis, plasmacytoma	Lytic lesion
		Perineural spread of parotid malignancy	...
Parotid space	VII	Salivary neoplasm	...
Jugular foramen	IX–XI	Paraganglioma	Erosion, vascularity, tendency to extend toward middle ear
Carotid space	IX–XII	Paraganglioma	Avid enhancement, vascularity
Sublingual space	XII	Carcinomas, salivary neoplasm	...

*CN I = olfactory nerve, CN II = optic nerve, CN IV = trochlear nerve, CN VI = abducens nerve.

Table 2: Imaging Features of CN Schwannomas

Imaging or Clinical Finding Category*	Imaging Feature
Nonenhanced T1-weighted MR imaging	Low to intermediate signal intensity
Contrast-enhanced T1-weighted MR imaging	Avid enhancement with or without nonenhancing cystic spaces
T2-weighted MR imaging	Heterogeneous high signal intensity
Nonenhanced CT	Low to intermediate attenuation
Contrast-enhanced CT	Variable enhancement
Slow growth pattern	Deformation of adjacent brain tissue, with disproportionately small amount of edema, given lesion size
	Smooth expansion of neural foramina
	Displacement of adjacent vessels without narrowing or occlusion
End-organ compromise	
Muscle denervation involving CNs III, IV, V3, VI, XI, and XII	Muscle edema, seen as high signal intensity with or without enlargement on T2-weighted MR images; or muscle atrophy with fat replacement, seen as high signal intensity and decreased muscle bulk on T1-weighted MR images
Vocal cord paresis involving CN X	Vocal cord medialization, atrophy

*CT = computed tomography, V3 = mandibular branch of CN V.
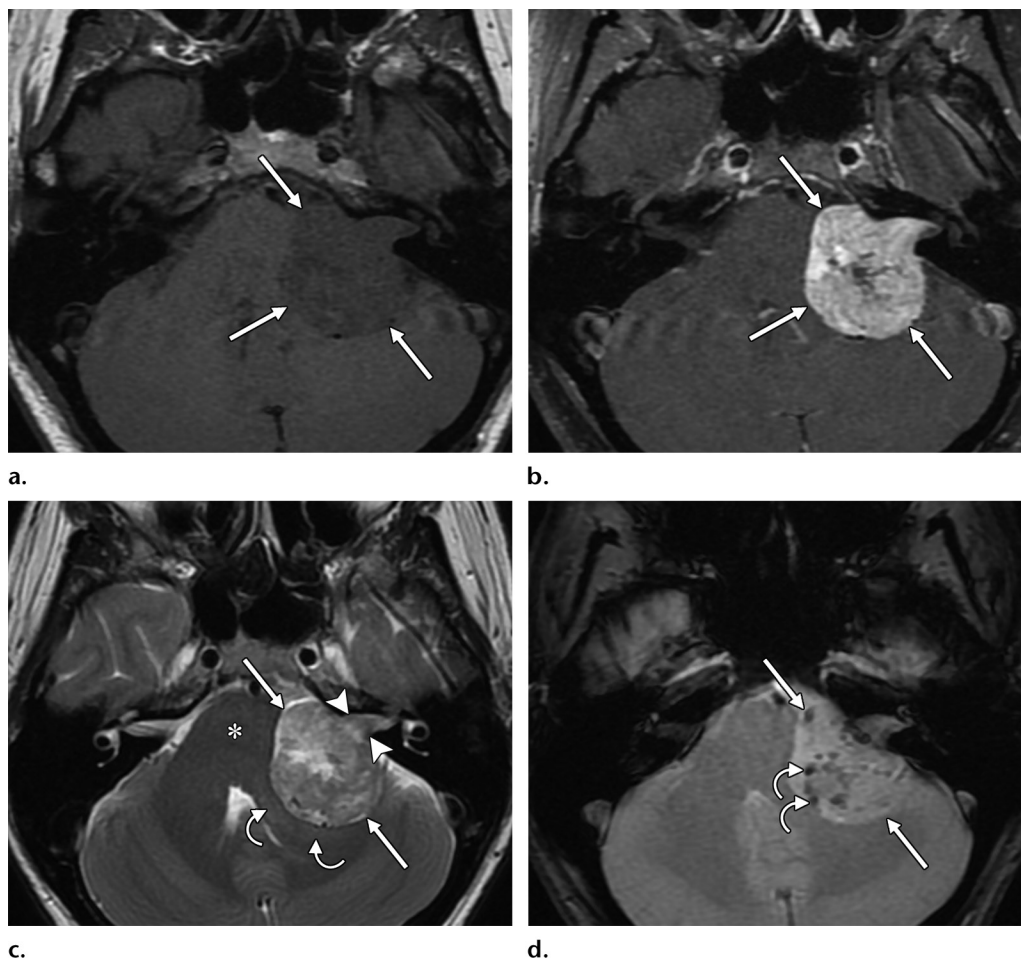
a.   b.

c.   d.

Figure 1.   Classic MR imaging appearances of CN VIII schwannoma in the cerebellopontine angle (CPA)–internal auditory canal (IAC) complex in a 46-year-old woman. The CN VIII schwannoma was proven at histopathologic analysis. **(a)** Axial T1-weighted MR image shows low to intermediate signal intensity of the mass (arrows). **(b)** Axial contrast-enhanced fat-suppressed T1-weighted MR image shows avid enhancement of the mass (arrows), which has an internal nonenhancing cystic focus. **(c)** Axial T2-weighted MR image shows heterogeneous high signal intensity of the schwannoma (straight arrows). The mass enlarges the porus acusticus internus (arrowheads) and exerts a mass effect on the brainstem (∗) and middle cerebellar peduncle (curved arrows), with a disproportionately small amount of edema, given the size of the mass. **(d)** Axial gradient-recalled-echo MR image shows the schwannoma (straight arrows) with foci of susceptibility artifact (curved arrows), which indicate intratumoral microhemorrhage.

CN owing to a long-standing mass effect. Second, the presence of a CN deficit is not diagnostic of CN schwannoma because other processes such as perineural spread of malignancy, which causes a similar deficit, may exert a mass effect on or invade the CN. In addition, schwannomas may arise from sympathetic branches along the carotid artery in the neck, cavernous sinus, and orbit in similar locations to the CNs.

Clinical Presentation

The clinical manifestations of CN schwannomas vary according to the nerve of origin and the location and size of the tumor; therefore, accurate imaging-based diagnosis is paramount. These tumors are often asymptomatic and discovered incidentally at imaging for an unrelated indication (18,19). If symptomatic, CN schwannomas

may cause symptoms resulting from their local mass effect, such as nausea and headache caused by brainstem compression. Alternatively, these tumors may result in symptoms that are related to specific CN deficits and that should guide a targeted search of the appropriate CNs (Table 3). For example, diplopia should direct the search to CN III, IV, and/or VI; facial numbness, paresthesias, or pain, to CN V; facial paresis, to CN VII; vertigo or hearing loss, to CN VIII; and dysphagia, dysphonia, or dysarthria, to CNs IX–XII.
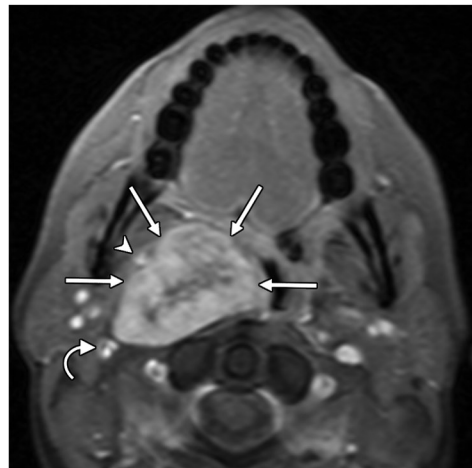
Anterior Cranial Fossa

The olfactory tract and bulb of CN I lie in the olfactory groove and send small penetrating nerves through the cribriform plate into the superior nasal cavity. Schwannomas arising from the anterior cranial fossa are rare, with only 33 cases
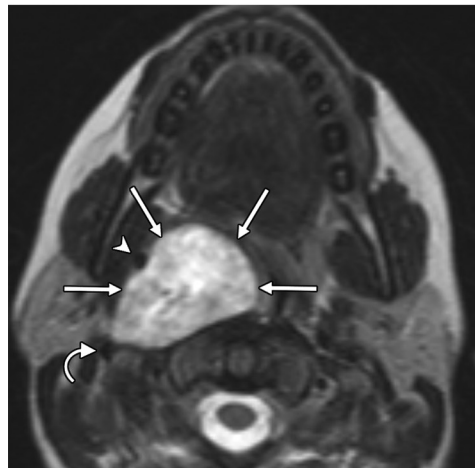
Figure 2. Histopathologically proven carotid space CN X schwannoma in a 32-year-old woman. **(a)** Axial contrast-enhanced CT image shows heterogeneous low to intermediate attenuation of the mass (straight arrows). The schwannoma splays the right ICA (arrowhead in **a–c**) and internal jugular vein (curved arrow in **a–c**). **(b)** Axial T2-weighted MR image shows heterogeneous high signal intensity of the mass (straight arrows). **(c)** Axial contrast-enhanced fat-suppressed T1-weighted MR image shows heterogeneous enhancement of the mass (straight arrows).

a.

b.   c.

reported in the literature as of 2011. However, these neoplasms have been found extending both superiorly into the anterior cranial fossa and inferiorly into the nasal cavity (20). Expected findings include osseous remodeling of the olfactory groove or nasal cavity (Fig 3).

It is important to recognize the aggressive features of sinonasal malignant neoplasms such as squamous cell carcinoma, sinonasal undifferentiated carcinoma, and esthesioneuroblastoma, which include bone destruction and invasion of the brain, orbit, or other surrounding structures. These features enable sinonasal malignant neoplasms to be distinguished from benign schwannomas (21).

Orbit

From the cavernous sinus, CN III, CN IV, the ophthalmic branch of CN V, and CN VI directly enter the orbit through the superior orbital fissure, whereas the maxillary branch of CN V courses through the foramen rotundum and superior pterygopalatine fossa to enter the orbit through the inferior orbital fissure. Therefore, schwannomas arising from these nerves may ap-

pear as a dumbbell-shaped mass spanning from the cavernous sinus to the orbit, with smooth expansion of the orbital fissures (Fig 4), or they may be confined to the orbit. Because CN II is myelinated by oligodendrocytes rather than schwann cells, rarely reported CN II schwannomas most likely arise from sympathetic fibers along the CN II sheath (12,22,23). If symptomatic, schwannomas in this region may cause proptosis, diplopia due to extraocular muscle compromise, vision loss due to a mass effect on CN II, or facial sensation disturbance due to ophthalmic or maxillary CN V branch involvement (12). Given the proximity of these nerves, it is often difficult to delineate the nerve of origin in this region, and evaluation for end-organ compromise can sometimes aid in this identification (Fig 4).

The most common orbital mass is cavernous malformation, which more commonly is homogeneously hyperintense on T2-weighted MR images and has enhancement that starts at a point and then spreads, in contrast to schwannoma, which has early widespread enhancement (24,25). If the

Table 3: Symptom-based Approach to Imaging Evaluation of CN Schwannomas

Symptom	CNs to Evaluate	Locations along CN Course to Evaluate*	End-organ Muscles to Evaluate for Possible Denervation*
Nasal congestion, fullness	I	Anterior cranial fossa, olfactory groove, superior nasal vault	…
Diplopia, vision loss from mass effect on CN II	III	Interpeduncular cistern, cavernous sinus, superior orbital fissure, orbit	Superior, inferior, and medial rectus muscles
	IV	Ambient cistern, cavernous sinus, superior orbital fissure, orbit	Superior oblique muscle
	VI	Prepontine cistern, Dorello canal, cavernous sinus, superior orbital fissure, orbit	Lateral rectus muscle
Facial numbness, tingling, pain	V	Prepontine cistern, Meckel cave, cavernous sinus (V1, V2), orbit (V1, V2), foramen rotundum (V2), foramen ovale (V3)	Muscles of mastication: masseter, temporalis, and pterygoid muscles (V3)
Facial paresis	VII	CPA cistern, IAC, temporal bone (labyrinthine, geniculate fossa, tympanic, mastoid segments), stylomastoid foramen, parotid space	…
Sensorineural hearing loss, vertigo	VIII	CPA cistern, IAC, cochlea, vestibule	…
Dysphagia, dysphonia, dysarthria, sensorineural hearing loss	IX	Cerebellomedullary cistern, jugular foramen, suprahyoid carotid space	…
No specific symptoms	X	Cerebellomedullary cistern, jugular foramen, suprahyoid and infrahyoid carotid spaces	Vocal cords
	XI	Cerebellomedullary cistern, jugular foramen, suprahyoid carotid space	Sternocleidomastoid and trapezius muscles
	XII	Cerebellomedullary cistern, hypoglossal canal, suprahyoid carotid space, mouth floor	Tongue muscles

*Data in parentheses are the specific branches of CN V that the given symptoms involve: V1 = ophthalmic branch of CN V, V2 = maxillary branch of CN V, V3 = mandibular branch of CN V.

patient has bone erosion, marrow replacement, and/or a personal history of malignancy, then perineural spread of neoplasm, direct invasion by a sinonasal tumor, and lymphoma need to be considered. Careful evaluation for the presence of a regional soft-tissue mass, lymphadenopathy, and abnormal bone marrow is critical.

Cavernous Sinus
The cavernous sinus contains CN III, CN IV, the ophthalmic and maxillary branches of CN V within its lateral wall, and CN VI alongside the ICA and sympathetic branches within its center. As mentioned earlier, all of these CNs course into the orbit by way of the orbital fissures, with the maxillary branch of CN V first coursing through the foramen rotundum into the pterygopalatine fossa. If symptomatic, schwannomas of this region may cause diplopia. A schwannoma may arise from any of these nerves within the cavernous si-

nus and cause it to have a convex contour, or if the tumor is large enough, it may extend in a dumbbell configuration through the orbital fissures and skull base foramina. Again, the proximity of these nerves makes the identification of the nerve of origin difficult, although correlation of the tumor location with the clinical history and evaluation for compromise of specific extraocular muscles may aid in the identification of the originating nerve.

The mandibular branch of CN V courses along the inferolateral margin of—not within—the cavernous sinus. Schwannomas arising from this branch can be confidently diagnosed on the basis of the characteristic extension through and expansion of the foramen ovale to course into the masticator and prestyloid parapharyngeal space. Resultant atrophy of the muscles of mastication may be seen (Fig 5).

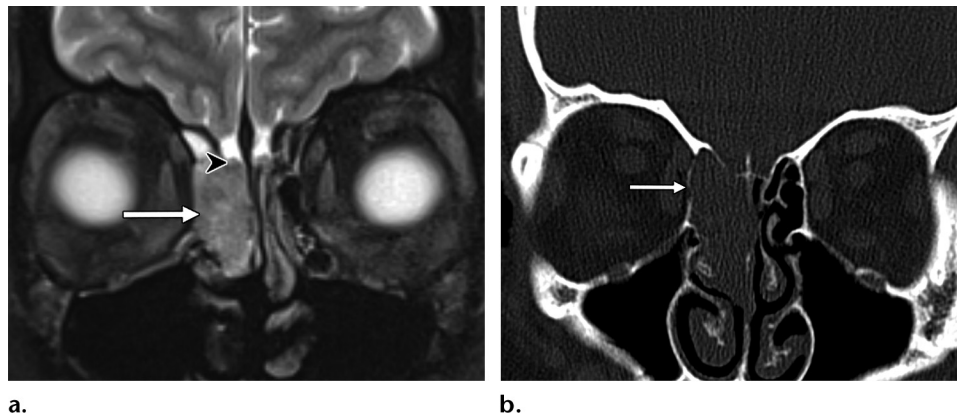As mentioned earlier, careful evaluation of the regional soft tissue and bone marrow is important

a.   b.

Figure 3. Histopathologically proven superior nasal cavity schwannoma in a 54-year-old man. **(a)** Coronal fat-suppressed T2-weighted MR image shows heterogeneous intermediate signal intensity of the mass (arrow). Note the close relationship of the mass with right CN I (arrowhead), just above the cribriform plate. **(b)** Coronal bone algorithm CT image shows expansile thinning of the adjacent lamina papyracea (arrow), without osseous destruction.
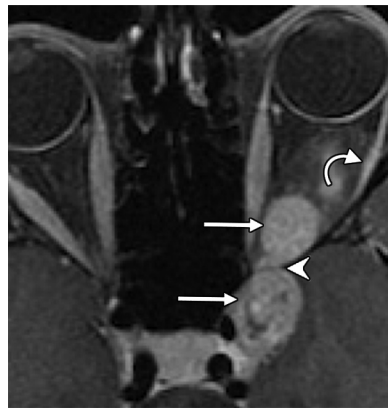

Figure 4. Histopathologically proven CN VI schwannoma in a 31-year-old woman. Axial contrast-enhanced fat-suppressed T1-weighted MR image shows a partially cystic, avidly enhancing dumbbell-shaped mass (straight arrows) extending from the left cavernous sinus to the orbital apex, through the expanded superior orbital fissure (arrowhead). Note the associated lateral rectus muscle atrophy (curved arrow), which suggests a CN VI origin. The CN VI origin was confirmed intraoperatively.

to exclude perineural spread of neoplasm and lymphoproliferative disorder. Furthermore, it is important to evaluate the adjacent cavernous ICA to avoid mistaking a lobular enhancing aneurysm for a schwannoma in this region. A cavernous sinus meningioma may simulate a schwannoma; however, meningioma often demonstrates an enhancing dural tail and has a greater propensity to narrow the cavernous ICA (26).

Intracranial Upper CNs III–VI

Intracranial upper CNs III–VI traverse the upper brainstem cisterns. CN III courses through the interpeduncular cistern into the cavernous sinus (Fig 6). CN IV is unique in that it is the only CN to arise from the dorsal brainstem, below the inferior colliculus of the midbrain, and then course around the lateral brainstem in the ambient cistern underneath the tentorium cerebelli on the way to the cavernous sinus (Fig 7). The prepontine cistern contains CN V on its way from the midlateral pons to the Meckel cave (Figs 8, 9) and CN VI traveling from the anterior pontomedullary junction to the Dorello ca-

nal (Fig 10). Therefore, the diagnostic approach for a patient with diplopia involves evaluation for CN schwannoma not only in the orbit and cavernous sinus but also in the interpeduncular, ambient, and prepontine cisterns and Dorello canal. Sizable schwannomas of the cisternal segments of these nerves have characteristic imaging features, as previously described (Table 2), and tend to deform the adjacent brainstem without invasion and with minimal edema, given the size of the lesions.

Enhancement of cisternal segments of the CNs may be seen with malignancies such as leptomeningeal spread of tumor, or with inflammatory conditions such as sarcoidosis. However, these conditions tend to involve multiple nerves and other meningeal surfaces, whereas schwannomas are more focal (27,28).

Intracranial and Intratemporal CNs VII–VIII

CN VII and CN VIII travel together from the lateral pontomedullary junction in the CPA through the IAC into the temporal bone, with CN VII anterior and superior to CN VIII. Schwannomas of these nerves may cause sensorineural hearing loss, vertigo, and/or hemifacial paresis or spasm. CN VIII is the most common CN of schwannoma involvement. CN VII and CN VIII schwannoma lesions classically appear
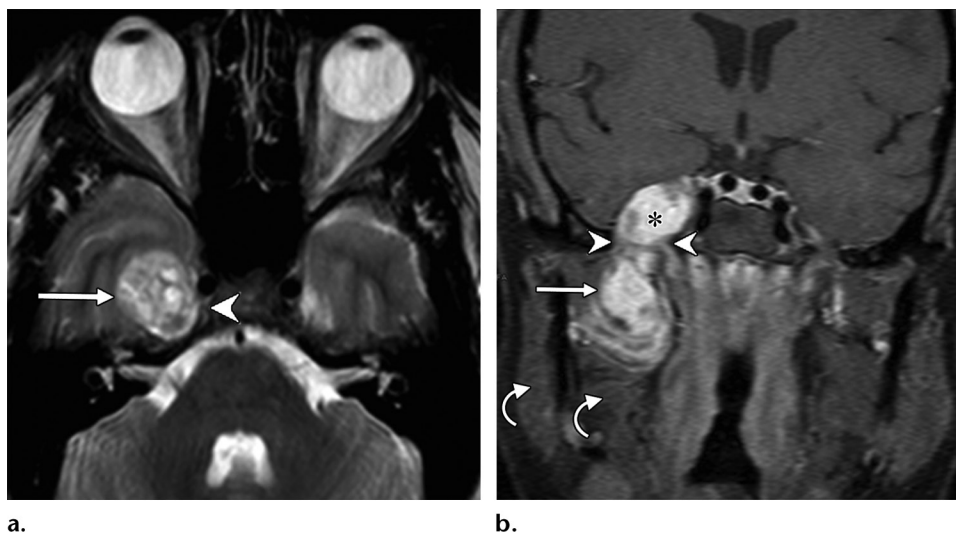
Figure 5. Histopathologically proven schwannoma of the mandibular branch of CN V in a 50-year-old woman. **(a)** Axial T2-weighted MR image shows a heterogeneously hyperintense mass (arrow) along the lateral right cavernous sinus (arrowhead) and Meckel cave. **(b)** Coronal contrast-enhanced fat-suppressed T1-weighted MR image shows a tubular heterogeneously enhancing schwannoma extending from the region of the Meckel cave (∗), through the expanded foramen ovale (arrowheads) into the masticator space (straight arrow). Note the associated atrophy of the right masseter and pterygoid muscles (curved arrows), which are innervated by the mandibular branch of CN V.
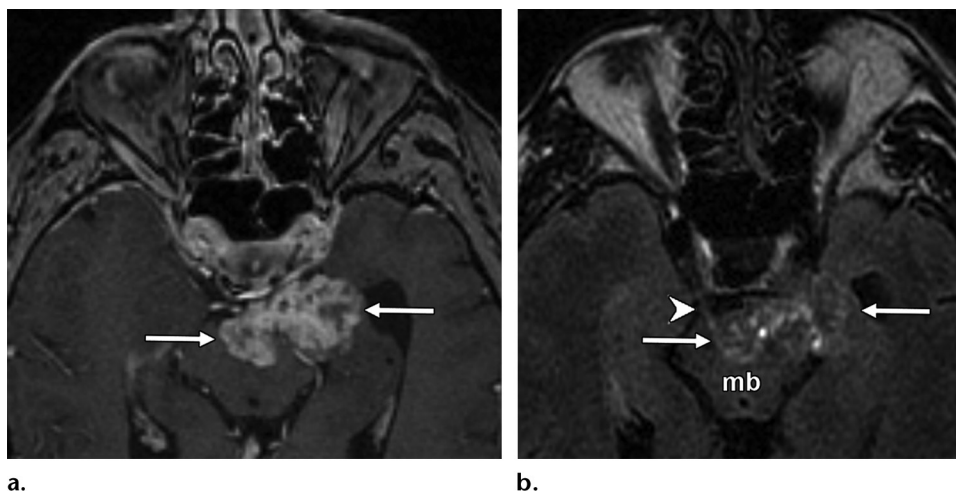

Figure 6. Histopathologically proven CN III schwannoma in a 66-year-old man. **(a)** Axial contrast-enhanced fat-suppressed T1-weighted MR image shows a large heterogeneously enhancing schwannoma (arrows) centered in the interpeduncular cistern region of CN III. **(b)** Axial fluid-attenuated inversion-recovery MR image shows the heterogeneous schwannoma (arrows) centered in the interpeduncular cistern, extending to the left along the course of the mandibular branch of CN V. Note the lack of edema in the deformed midbrain *(mb)* and left medial temporal lobe. The anatomy of contralateral CN III (arrowhead) can be seen arising from the ventral midbrain and coursing through the interpeduncular cistern into the cavernous sinus.

as an "ice cream cone"–shaped mass in the CPA cistern and IAC, with expansion of the IAC and porus acusticus (Fig 1). Intralabyrinthine schwannoma, a rare variant of CN VIII schwannoma, may be seen as a focus of enhancement in the cochlea or vestibule on contrast-enhanced T1-weighted MR images, with a corresponding hypointense filling defect on thin-section steady-state free precession or other T2-weighted MR images (29,30).

Although CN VII and CN VIII schwannomas may have identical imaging appearances if they are confined to the CPA-IAC complex, it is important to evaluate the findings for extended enhancement or expansion of the labyrinthine segment and geniculate ganglion of CN VII (Fig 11), as this is a subtle clue to a CN VII rather than CN VIII origin. The geniculate fossa is the most common CN VII segment involved with schwannoma (31). The intratemporal CN VII
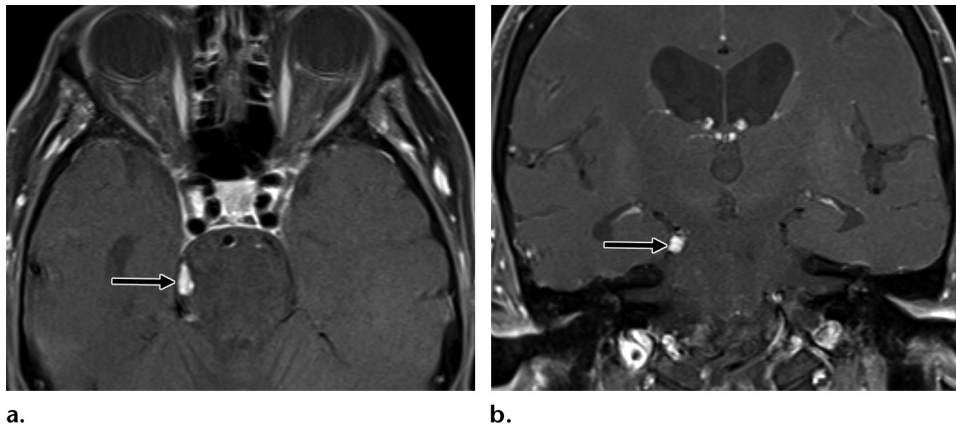
a.   b.

Figure 7. Clinically diagnosed CN IV schwannoma in an 83-year-old woman who presented with diplo-pia and CN IV palsy. **(a)** Axial contrast-enhanced fat-suppressed T1-weighted MR image shows a homo-geneously enhancing schwannoma (arrow) in the ambient cisternal segment of right CN IV. **(b)** Coronal contrast-enhanced fat-suppressed T1-weighted MR image shows the enhancing schwannoma (arrow) in the right ambient cisternal segment, underneath the tentorium.
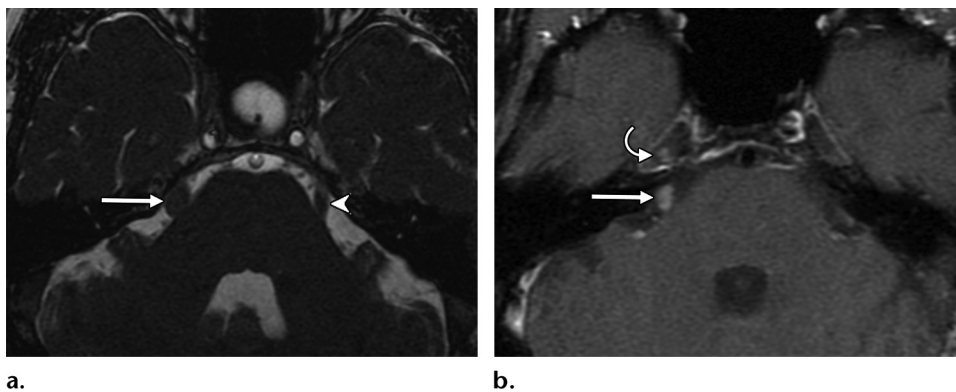

a.   b.

Figure 8. Small clinically diagnosed CN V schwannoma in a 64-year-old man. **(a)** Axial fast imaging employing steady-state acquisition MR image shows expansion of the cisternal segment of right CN V (arrow). The contralateral CN V (arrowhead), which has a normal anatomy, exits the lateral pons and courses through the prepontine cistern into the Meckel cave. **(b)** Axial contrast-enhanced fat-suppressed T1-weighted MR image shows an enhancing right cisternal CN V schwannoma (straight arrow), with extension into the Meckel cave (curved arrow).
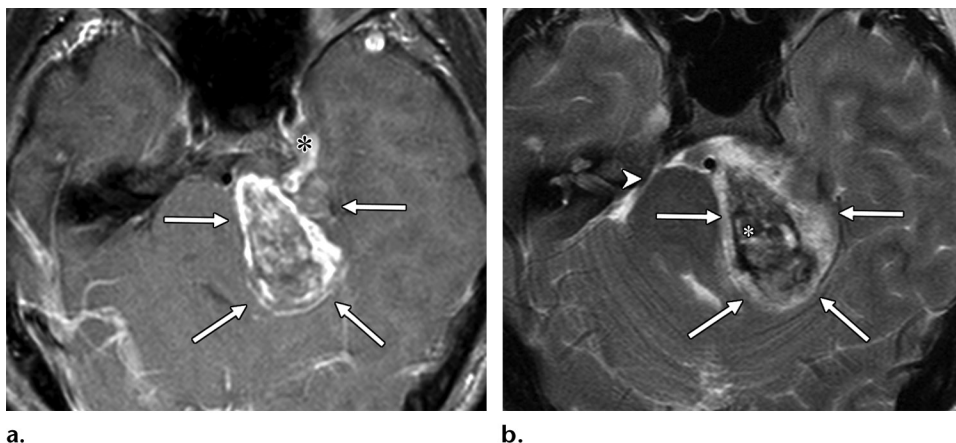

a.   b.

Figure 9. Large histopathologically proven CN V schwannoma in a 19-year-old man. **(a)** Axial contrast-enhanced fat-suppressed T1-weighted MR image shows a large heterogeneously enhancing schwannoma (arrows) in the prepontine cistern. The schwannoma has mass effect on the brainstem and extends into the left Meckel cave (∗). **(b)** Axial T2-weighted MR image shows that the schwannoma (arrows) contains hypointense areas (∗), which indicate hemorrhage. Note the appearance and course of the contralateral CN V (arrowhead) for comparison.
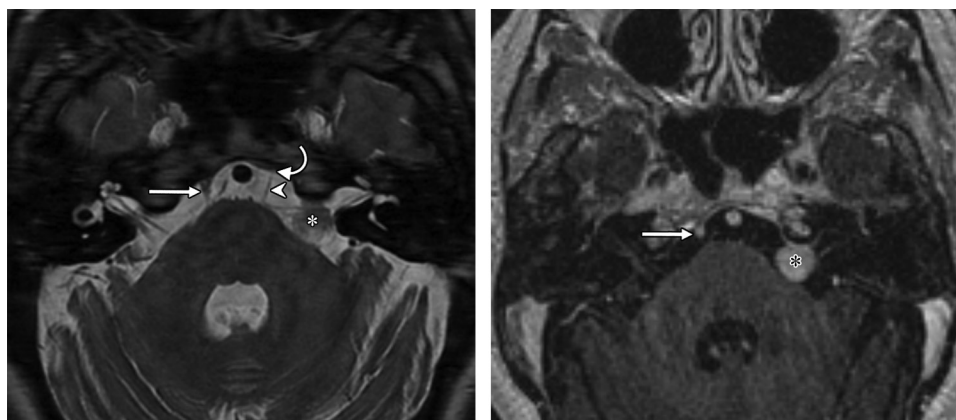
a.   b.

Figure 10.   Clinically diagnosed CN VI schwannoma and lower CN schwannoma in a 67-year-old woman. **(a)** Axial T2-weighted MR image shows asymmetric enlargement of the distal cisternal segment of right CN VI (straight arrow) as it enters the Dorello canal. The contralateral CN VI cisternal segment (arrowhead) is coursing from the ventral pons through the prepontine cistern into the Dorello canal (curved arrow). A larger left lower CN schwannoma (∗) is present. **(b)** Axial contrast-enhanced T1-weighted MR image shows enhancement of both the small right CN VI schwannoma (arrow) and larger left lower CN schwannoma (∗).

schwannomas are seen smoothly expanding the bone canal of the involved segments at high-resolution CT of the temporal bone and exhibit the characteristic T2-prolongation and enhancement at MR imaging (Figs 12, 13) (13,31).

The differential diagnosis for enhancing CPA tumors includes meningioma, which may extend into the IAC, although it often demonstrates an enhancing dural tail. Intratemporal lesions that may occur along the course of CN VII include hemangiomas, cholesteatomas, bone lesions (metastasis, plasmacytoma), and perineural spread of parotid malignancy (13). Osseous metastasis and cholesteatoma commonly cause lytic bone destruction. CN VII hemangiomas commonly occur at the geniculate fossa, have irregular borders with intralesional stippled calcifications, and cause facial paralysis despite their relatively small size at presentation (32,33). Finally, it is paramount to recognize the perineural spread of head and neck cancers that affect CN VII by performing a careful evaluation of the regional soft tissue (34).

## Intracranial and Skull Base Foraminal Lower CNs IX–XII

CN IX, CN X, and CN XI arise sequentially from the postolivary sulcus of the lateral medulla, traverse the cerebellomedullary cisterns, and then exit through the jugular foramen (Fig 14). CN XII arises from the preolivary sulcus and exits through the hypoglossal canal (Fig 15). Therefore, the lower CN schwannomas occur in the cerebellomedullary cistern as a tubular or dumbbell-shaped enhancing mass that extends into and expands the jugular foramen (CN IX–XI schwannomas) (Fig 14)

or hypoglossal canal (CN XII schwannoma) (Fig 15) (14,35). A schwannoma involving the hypoglossal canal clearly indicates a CN XII origin, whereas a schwannoma in the cerebellomedullary cistern and jugular foramen can originate from any among lower CNs IX–XI. The clinical presentation varies according to the CN of origin and local mass effect. Owing to the slow growth and clinical silence of these tumors, they are usually large at presentation and commonly cause sensorineural hearing loss that results from their mass effect on adjacent CN VIII (14,36,37). The associated end-organ compromise is usually a late finding and includes paresis of the vocal cord (related to CN X schwannoma), atrophy of the trapezius or sternocleidomastoid muscles (related to CN XI schwannoma), and atrophy of the tongue muscles (related to CN XII schwannoma) on the ipsilateral side. Denervation-induced muscle atrophy is most apparent on non–fat-suppressed T1-weighted MR images as high signal intensity related to fat replacement of muscle fibers and decreased muscle bulk (Fig 5).

The most common tumor of the jugular foramen is glomus jugulare paraganglioma. Although schwannomas grow superomedially along the course of the CN toward the brainstem (Fig 14), glomus jugulare tumors grow superolaterally toward the floor of the middle ear (38,39). At CT, glomus jugulare paraganglioma classically involves permeative erosion of the jugular spine and adjacent petrous and mastoid segments of the temporal bone, and this erosion enables the differentiation of paraganglioma from schwannoma, which involves smooth well-corticated osseous remodeling. On MR images, paragangli-
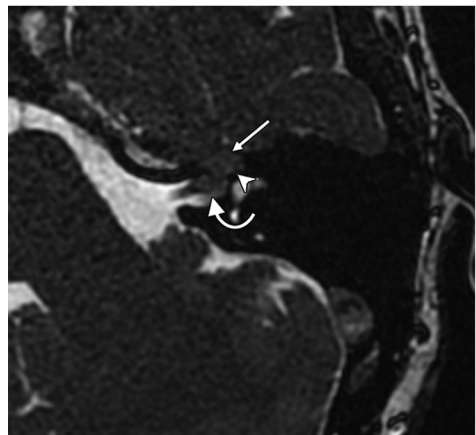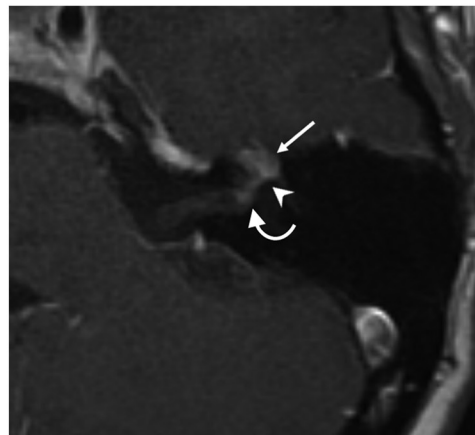
Figure 11. Small clinically diagnosed CN VII schwannoma in a 24-year-old woman. **(a)** Axial CT image shows the anatomy of the right CN VII labyrinthine segment (arrowhead) and geniculate fossa (dashed arrow). The left geniculate fossa (solid arrow) is expanded. **(b)** Axial fast imaging employing steady-state acquisition MR image shows neoplastic tissue expanding the distal CN VII canalicular segment (curved arrow) and extending into and expanding the labyrinthine segment (arrowhead) and geniculate segment (straight arrow). **(c)** Axial contrast-enhanced T1-weighted MR image shows corresponding enhancement of the canalicular (curved arrow), labyrinthine (arrowhead), and geniculate (straight arrow) segments of CN VII.

a.

b.　　　　　　　　　　　　　　　　　　　c.
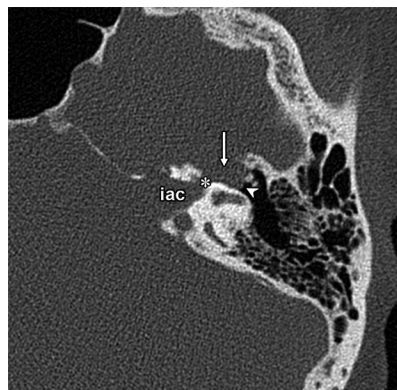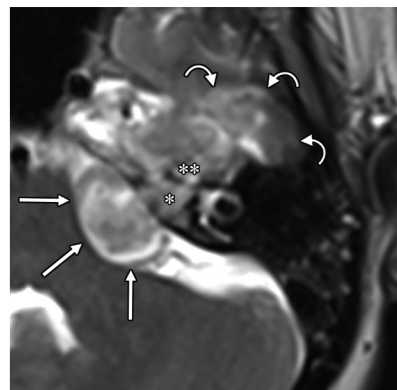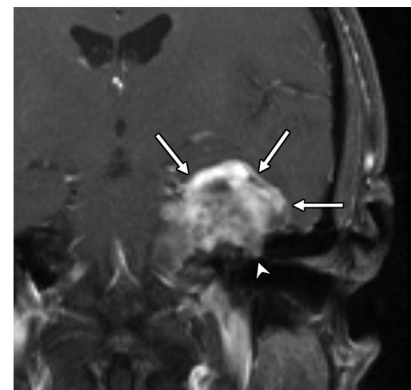
a.　　　　　　　　　　　　b.　　　　　　　　　　　　c.

Figure 12. Large histopathologically proven CN VII schwannoma in a 54-year-old woman. **(a)** Axial temporal bone CT image shows expansion of the IAC *(iac)*, CN VII labyrinthine segment (∗), geniculate fossa (arrow), and proximal tympanic segment (arrowhead), without osseous destruction. **(b)** Axial T2-weighted MR image shows a large lobulated heterogeneously hyperintense schwannoma spanning from the CPA cistern (straight arrows) through the labyrinthine (∗) and geniculate (∗∗) segments and bulging into the middle cranial fossa (curved arrows). Note the lack of edema in the adjacent brain tissue, which indicates slow growth. **(c)** Coronal contrast-enhanced fat-suppressed T1-weighted MR image shows heterogeneous enhancement of the schwannoma, which is bulging into the middle cranial fossa (arrows) and inferiorly into the middle ear tympanic segment (arrowhead).

oma exhibits the characteristic "salt and pepper" pattern caused by the high signal intensity of subacute hemorrhage or slow flow and the low signal intensity of flow voids, with intense enhancement related to hypervascularity (39).

Extracranial CN Schwannomas

Parotid Space
After its temporal bone course, CN VII exits the stylomastoid foramen and courses through the
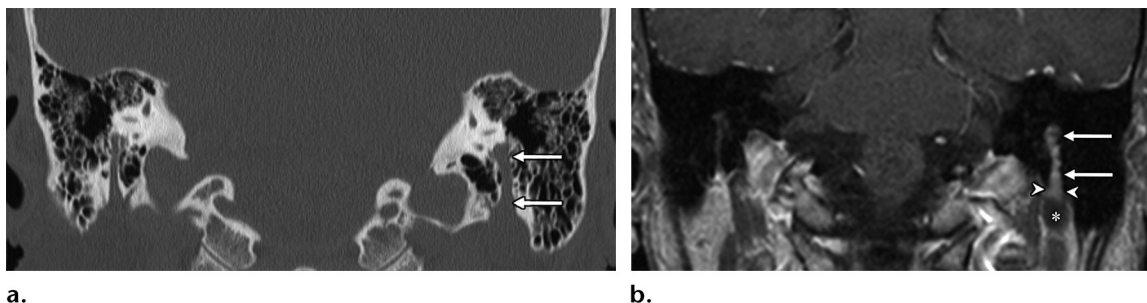
Figure 13. Clinically diagnosed mastoid segment CN VII schwannoma in a 62-year-old woman. **(a)** Coronal temporal bone CT image shows asymmetric enlargement of the left mastoid segment of CN VII (arrows). **(b)** Coronal contrast-enhanced T1-weighted MR image shows an enhancing schwannoma in the expanded left mastoid segment (arrows), with a nonenhancing cystic portion (∗) bulging out of the stylomastoid foramen (arrowheads).
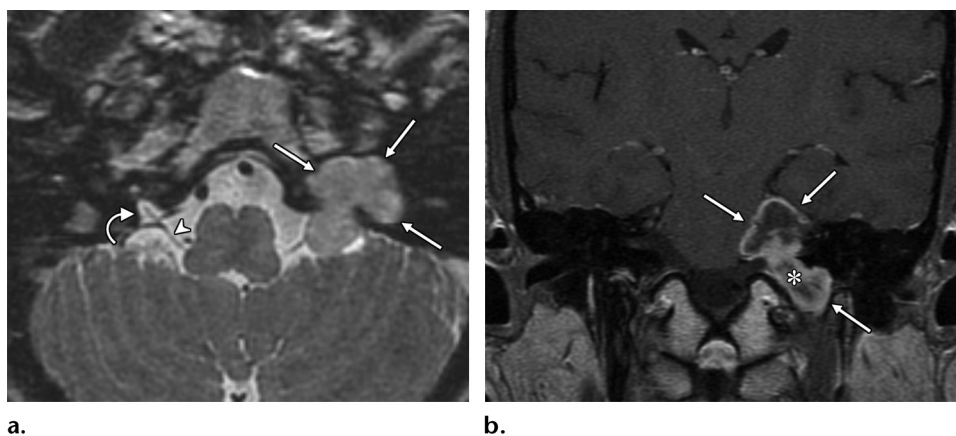

Figure 14. Clinically diagnosed jugular foramen lower CN schwannoma in a 44-year-old man. **(a)** Axial T2-weighted MR image shows the anatomy of the right CN IX–X course (arrowhead). Right CNs IX–X arise from the postolivary sulcus in the cerebellomedullary cistern and course into the right jugular foramen (curved arrow). The dumbbell-shaped hyperintense schwannoma is expanding the left jugular foramen (straight arrows) and extending from the cisternal segment in the cerebellomedullary cistern. **(b)** Coronal contrast-enhanced T1-weighted MR image shows a heterogeneously enhancing, partially cystic schwannoma (arrows) extending into and expanding the left jugular foramen (∗). The vector of growth is superomedially toward the brainstem, along the course of the nerve.

Figure 15. Clinically diagnosed CN XII schwannoma in a 29-year-old woman with neurofibromatosis type 2. Axial contrast-enhanced T1-weighted MR image shows a homogeneously enhancing schwannoma (arrows) extending into the right hypoglossal canal (∗).
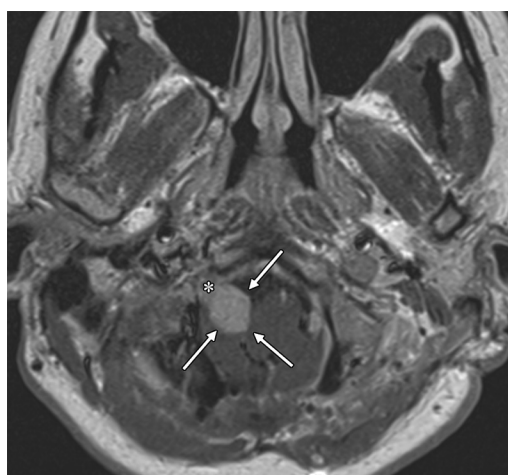
parotid gland laterally to the retromandibular vein. Intraparotid CN VII schwannomas demonstrate well-defined lobular or tubular margins and occur along the main trunk of CN VII, coursing posterolaterally to the retromandibular vein and extending toward or into the expanded stylomastoid foramen (Fig 16) (19). Alternatively, a CN VII schwannoma may be confined to the parotid gland and resemble the more commonly encountered benign mixed tumor. A parotid lesion with ill-defined margins should be promptly recognized as a parotid malignancy, and although CN VII palsy may occur with schwannoma, this clinical finding should also raise suspicion for malignancy (40).

Carotid Space

After exiting the skull base, lower CNs IX–XII course together in the carotid space and branch off to innervate the tongue, pharynx, larynx, and trapezius and sternocleidomastoid muscles. After
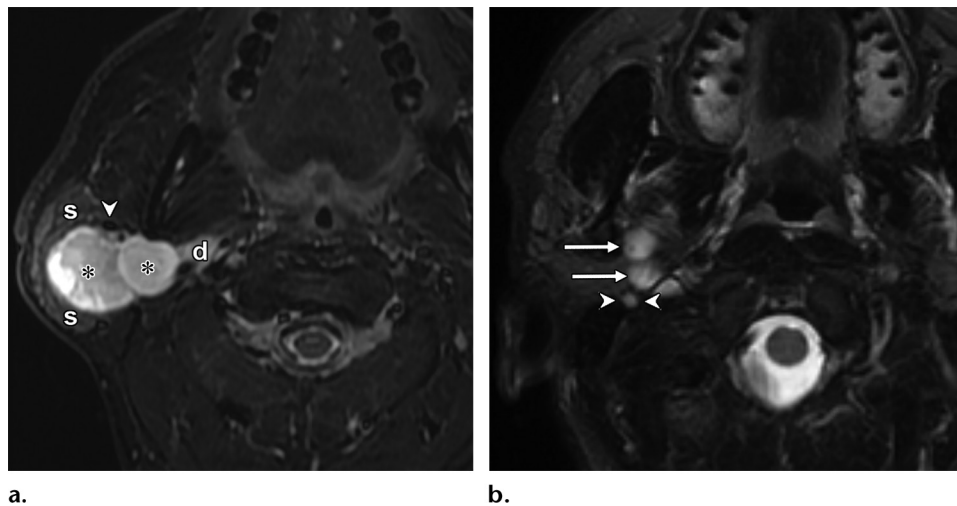
a.　　　　　　　　　　　　　　　　**b.**

Figure 16. Histopathologically proven parotid space CN VII schwannoma in a 40-year-old man. **(a)** Axial short τ inversion-recovery MR image shows a tubular hyperintense schwannoma (*) posterior to the retromandibular vein (arrowhead) and extending from the region of the deep lobe *(d)* of the parotid gland to the superficial lobe *(s)*, along the course of CN VII. **(b)** Axial short τ inversion-recovery MR image shows the superior portion of the schwannoma (arrows) extending into the stylomastoid foramen (arrowheads).
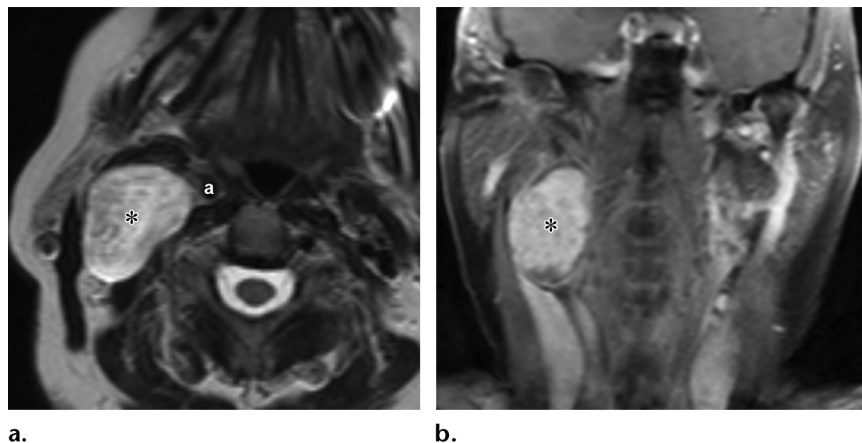

a.　　　　　　　　　　　　　　　　**b.**

Figure 17. Histopathologically proven carotid space schwannoma in a 64-year-old man. **(a)** Axial T2-weighted MR image shows a large heterogeneously hyperintense schwannoma (*) in the right carotid space, displacing the ICA *(a).* **(b)** Coronal contrast-enhanced fat-suppressed T1-weighted MR image shows avid enhancement of the mass (*).

coursing briefly in the suprahyoid carotid space, CN IX exits anteriorly, dividing into pharyngeal, tonsillar, and lingual branches, and CN XI exits posteriorly to the posterior triangle. CN XII courses more inferiorly in the suprahyoid carotid space between the ICA and internal jugular vein, and exits the carotid sheath at the posterior belly of the digastric muscle, terminating in the sublingual space. Although CNs IX–XII all course through the upper suprahyoid carotid space at the level of the nasopharynx, only CN X continues farther inferiorly in the infrahyoid carotid space. Therefore, an infrahyoid carotid space schwannoma can be attributed to a CN X origin (41).

Schwannomas of the carotid space share imaging features with schwannomas in other locations, and it should be noted that they tend to displace the ICA anteromedially at the nasopharynx and splay the ICA and internal jugular vein in opposite directions (Figs 2, 17) (16,17). Conversely, a sympathetic chain schwannoma, which arises adjacent to the carotid sheath, tends to displace both the ICA and internal jugular vein in the same direction (16,17). Paragangliomas (glomus jugulare, glomus vagale, and carotid body tumor) can be distinguished from schwannomas on the basis of their serpiginous hypervascularity, which is not typically found in schwannomas (39).

Sublingual Space

CN XII courses from the hypoglossal canal to the sublingual space to innervate the tongue. CN XII schwannomas along the mouth floor may appear as well-defined round or tubular lesions
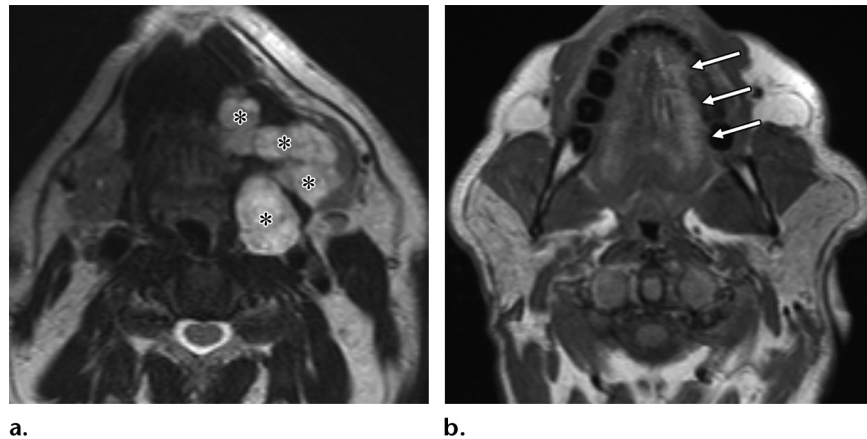
Figure 18. Histopathologically proven CN XII schwannoma along the mouth floor in a 51-year-old man. **(a)** Axial T2-weighted MR image shows a tubular hyperintense schwannoma (∗) along the lingual branch of CN XII. **(b)** Axial T1-weighted MR image shows an asymmetric hyperintensity in the left hemitongue musculature (arrows), indicating denervation atrophy.

that are hyperintense on T2-weighted MR images (Fig 18). Associated hemitongue atrophy may be present as evidence of the end-organ compromise, which may appear as an asymmetric area of high signal intensity in the ipsilateral hemitongue musculature on T1-weighted MR images (Fig 18). Ill-defined margins of a lesion in this space should be recognized to indicate an aggressive lesion such as squamous cell carcinoma or salivary gland malignancy.

Conclusion

CN schwannomas may arise along the course of any of the CNs, including the cisternal, skull base, and extracranial segments of the head and neck. Knowledge of the CN anatomy and imaging features of schwannoma is the foundation of an accurate diagnosis. Although vestibular schwannomas commonly cause hearing loss related to the deficit of the originating CN, large schwannomas commonly cause neurologic symptoms related to their local mass effect. At times, imaging evidence of end-organ compromise can aid in the identification of the originating CN or serve as a prognostic indicator of the risk of treatment-related CN palsy. With a detailed understanding of the imaging features and clinical manifestations of CN schwannomas, the radiologist can have a key role in the diagnosis of CN schwannomas and the treatment planning for affected patients.

References

1. Wippold FJ 2nd, Lubner M, Perrin RJ, Lämmle M, Perry A. Neuropathology for the neuroradiologist: Antoni A and Antoni B tissue patterns. AJNR Am J Neuroradiol 2007;28(9):1633–1638.
2. Luo B, Sun G, Zhang B, Liang K, Wen J, Fang K. Neuroradiological findings of intracranial schwannomas not arising from the stems of CNs. Br J Radiol 2004;77(924): 1016–1021.
3. Sarma S, Sekhar LN, Schessel DA. Nonvestibular schwannomas of the brain: a 7-year experience. Neurosurgery 2002;50(3):437–448; discussion 438–439.
4. Fisher LM, Doherty JK, Lev MH, Slattery WH 3rd. Distribution of nonvestibular CN schwannomas in neurofibromatosis 2. Otol Neurotol 2007;28(8):1083–1090.
5. Thomas AK, Egelhoff JC, Curran JG, Thomas B. Pediatric schwannomatosis, a rare but distinct form of neurofibromatosis. Pediatr Radiol 2016;46(3):430–435.
6. Sheth S, Branstetter BF 4th, Escott EJ. Appearance of normal CNs on steady-state free precession MR images. RadioGraphics 2009;29(4):1045–1055.
7. Blitz AM, Choudhri AF, Chonka ZD, et al. Anatomic considerations, nomenclature, and advanced cross-sectional imaging techniques for visualization of the CN segments by MR imaging. Neuroimaging Clin N Am 2014;24(1):1–15.
8. Moon WJ, Roh HG, Chung EC. Detailed MR imaging anatomy of the cisternal segments of the glossopharyngeal, vagus, and spinal accessory nerves in the posterior fossa: the use of 3D balanced fast-field echo MR imaging. AJNR Am J Neuroradiol 2009;30(6):1116–1120.
9. Koga H, Matsumoto S, Manabe J, Tanizawa T, Kawaguchi N. Definition of the target sign and its use for the diagnosis of schwannomas. Clin Orthop Relat Res 2007;464: 224–229.
10. Thamburaj K, Radhakrishnan VV, Thomas B, Nair S, Menon G. Intratumoral microhemorrhages on T2*-weighted gradient-echo imaging helps differentiate vestibular schwannoma from meningioma. AJNR Am J Neuroradiol 2008;29(3):552–557.
11. Sriskandan N, Connor SEJ. The role of radiology in the diagnosis and management of vestibular schwannoma. Clin Radiol 2011;66(4):357–365.
12. Kapur R, Mafee MF, Lamba R, Edward DP. Orbital schwannoma and neurofibroma: role of imaging. Neuroimaging Clin N Am 2005;15(1):159–174.
13. Chung SY, Kim DI, Lee BH, Yoon PH, Jeon P, Chung TS. Facial nerve schwannomas: CT and MR findings. Yonsei Med J 1998;39(2):148–153.
14. Eldevik OP, Gabrielsen TO, Jacobsen EA. Imaging findings in schwannomas of the jugular foramen. AJNR Am J Neuroradiol 2000;21(6):1139–1144.
15. Stangerup S-E, Caye-Thomasen P, Tos M, Thomsen J. The natural history of vestibular schwannoma. Otol Neurotol 2006;27(4):547–552.
16. Anil G, Tan TY. Imaging characteristics of schwannoma of the cervical sympathetic chain: a review of 12 cases. AJNR Am J Neuroradiol 2010;31(8):1408–1412.
17. Nagamine WH, Conneely MF, Petruzzelli GJ, Hacein-Bey L. Glossopharyngeal schwannoma of the suprahyoid carotid

space: case report and discussion of the relationship to the carotid artery. Laryngoscope 2009;119(4):653–656.

18. Biswas D, Marnane CN, Mal R, Baldwin D. Extracranial head and neck schwannomas: a 10-year review. Auris Nasus Larynx 2007;34(3):353–359.

19. Shimizu K, Iwai H, Ikeda K, Sakaida N, Sawada S. Intraparotid facial nerve schwannoma: a report of five cases and an analysis of MR imaging results. AJNR Am J Neuroradiol 2005;26(6):1328–1330.

20. Figueiredo EG, Soga Y, Amorim RL, Oliveira AM, Teixeira MJ. The puzzling olfactory groove schwannoma: a systematic review. Skull Base 2011;21(1):31–36.

21. Loevner LA, Sonners AI. Imaging of neoplasms of the paranasal sinuses. Neuroimaging Clin N Am 2004;14(4):625–646.

22. Ramey WL, Arnold SJ, Chiu A, Lemole M. A rare case of optic nerve schwannoma: case report and review of the literature. Cureus 2015;7(4):e265.

23. Kim DS, Choi JU, Yang KH, Jung JM. Optic sheath schwannomas: report of two cases. Childs Nerv Syst 2002;18 (12):684–689.

24. Meltzer DE. Orbital imaging: a pattern-based approach. Radiol Clin North Am 2015;53(1):37–80.

25. Xian J, Zhang Z, Wang Z, et al. Evaluation of MR imaging findings differentiating cavernous haemangiomas from schwannomas in the orbit. Eur Radiol 2010;20(9):2221–2228.

26. Shaffrey ME, Dolenc VV, Lanzino G, Wolcott WP, Shaffrey CI. Invasion of the internal carotid artery by cavernous sinus meningiomas. Surg Neurol 1999;52(2):167–171.

27. Collie DA, Brush JP, Lammie GA, et al. Imaging features of leptomeningeal metastases. Clin Radiol 1999;54(11):765–771.

28. Saremi F, Helmy M, Farzin S, Zee CS, Go JL. MRI of CN enhancement. AJR Am J Roentgenol 2005;185(6):1487–1497.

29. Salzman KL, Childs AM, Davidson HC, Kennedy RJ, Shelton C, Harnsberger HR. Intralabyrinthine schwannomas: imaging diagnosis and classification. AJNR Am J Neuroradiol 2012;33(1):104–109.

30. Donnelly MJ, Daly CA, Briggs RJ. MR imaging features of an intracochlear acoustic schwannoma. J Laryngol Otol 1994;108(12):1111–1114.

31. Wiggins RH 3rd, Harnsberger HR, Salzman KL, Shelton C, Kertesz TR, Glastonbury CM. The many faces of facial nerve schwannoma. AJNR Am J Neuroradiol 2006;27(3):694–699.

32. Mijangos SV, Meltzer DE. Case 171: facial nerve hemangioma. Radiology 2011;260(1):296–301.

33. Semaan MT, Slattery WH, Brackmann DE. Geniculate ganglion hemangiomas: clinical results and long-term follow-up. Otol Neurotol 2010;31(4):665–670.

34. Raghavan P, Mukherjee S, Phillips CD. Imaging of the facial nerve. Neuroimaging Clin N Am 2009;19(3):407–425.

35. Leonetti JP, Anderson DE, Marzo SJ, Origitano TC, Shirazi M. Intracranial schwannomas of the lower CNs. Otol Neurotol 2006;27(8):1142–1145.

36. Sedney CL, Nonaka Y, Bulsara KR, Fukushima T. Microsurgical management of jugular foramen schwannomas. Neurosurgery 2013;72(1):42–46; discussion 46.

37. Sanna M, Bacciu A, Falcioni M, Taibah A. Surgical management of jugular foramen schwannomas with hearing and facial nerve function preservation: a series of 23 cases and review of the literature. Laryngoscope 2006;116(12):2191–2204.

38. Macdonald AJ, Salzman KL, Harnsberger HR, Gilbert E, Shelton C. Primary jugular foramen meningioma: imaging appearance and differentiating features. AJR Am J Roentgenol 2004;182(2):373–377.

39. Vogl TJ, Bisdas S. Differential diagnosis of jugular foramen lesions. Skull Base 2009;19(1):3–16.

40. Veillona F, Ramos-Taboada L, Abu-Eid M, Charpiot A, Riehm S. Imaging of the facial nerve. Eur J Radiol 2010;74(2):341–348.

41. Ong CK, Chong VFH. The glossopharyngeal, vagus and spinal accessory nerves. Eur J Radiol 2010;74(2):359–367.